15TH IEA HEAT PUMP CONFERENCE
MAY 26–29, 2026 | HOFBURG
VIENNA 2026
DECARBONISATION THROUGH INNOVATION

Enhancing heat transfer in ground collectors using internal fins

Niklas Hidman[a], Daniel Almgren[b], Kim Johansson[b], Eskil Nilsson[c]

[a]Division of Fluid Dynamics, Chalmers University of Technology, Gothenburg, SE-412 96, Sweden
[b]MuoviTech Sweden AB, Bramhult, SE-507 30, Sweden
[c]Ernstromgruppen AB, Gothenburg, SE-411 10, Sweden

Abstract

We evaluate, using fully resolved Direct Numerical Simulations (DNS), the thermohydraulic performance of geothermal collector pipes with internal surface modifications (fins). The purpose of the fins is to enhance the convective heat transfer of the brine without significantly increasing the pressure drop. Due to fluctuating demands, geothermal heat pumps operate at varying heat loads, often regulated using the brine circulation pump. This regulation gives brine flow rates and typical Reynolds numbers in the range $1300 < Re < 3300$, where the transition to turbulence for smooth pipes is at approximately $Re = 2300$. Consequently, the brine is operated in both laminar and unsteady flow conditions. During laminar flow, the brine convective heat transfer resistance is a major contribution (≈50%) of the borehole thermal resistance. At turbulent conditions, the convective resistance is, however, very small compared to the borehole resistance. A suitable fin design in the collector pipes should thus trigger an unsteady flow at $Re < 2300$, without significantly increasing the pressure drop at $Re > 2300$ (that decreases system efficiency). Here, we use DNS to find a fin design that achieves both objectives. We start by evaluating three fin design strategies; straight axial fins; helical fins continuously rotating around the pipe axis; and fins rotating in alternating directions around the pipe axis. We also assess the influence of the fin size, the number of fins and their twist rate on the heat transfer rate and pressure drop. We find a promising design of alternating helical fins that triggers an unsteady flow down to about $Re = 1700$. This design enhances the heat transfer rate by 300-600% in the range of $1700 < Re < 2300$ compared to a smooth pipe with only minor increase in the pressure drop (max about 2%) outside of this range.

Keywords: geothermal collector; internally finned pipe; heat transfer enhancement; turbulence trigger; DNS.

1. Introduction

Geothermal systems with vertical ground heat exchangers (VGHEs) involve high investment costs, mainly due to drilling [1]. Borehole depth and diameter depend on the borehole thermal resistance (resistance between the brine and the borehole wall) [2, 3]. Lowering this resistance can reduce drilling costs and improve overall system performance [2]. A practical approach is to decrease the convective resistance within the collector pipe, which also lowers the effective grout resistance by evening out the pipe wall temperature, further enhancing system efficiency [4]. Consequently, improving the thermohydraulic performance of collector pipes can substantially enhance efficiency and reduce investment costs in geothermal systems [1, 4–6].

Heat transfer enhancement methods in heat exchanger pipes are generally classified as active or passive [7, 8]. Active methods require external power and complex designs, making them unsuitable for underground collector pipes operating maintenance-free for decades. Passive methods, involving surface or geometric pipe modifications, are thus more suitable for the present application. These approaches enhance convection and increase the effective heat transfer area.

Ribs and fins are especially attractive due to their proven effectiveness and manufacturability [9] and strong thermohydraulic performance [10]. Given that geothermal collector pipes are typically hundreds of meters long, modifications must be cheap and easy to manufacture, or deeper drilling remains more economical [4]. This work therefore investigates the use of continuous internal fins or ribs that allow for non-intermittent production processes. The performance of continuous internal fins has been widely studied before (see [8, 10]). However, geothermal systems impose unique practical constraints, requiring tailored fin designs that balance thermal performance, pressure drop, and manufacturability. In the latter constraint, the fins should be compatible with standard plastic pipe extrusion. Therefore, this study focuses on pipes with a constant cross-section that may rotate slightly along the axis.

Geothermal heat pumps operate under varying loads due to hourly to seasonal fluctuations. Inverter-controlled circulation pumps adjust the brine flow, resulting in Reynolds numbers $Re = U_b D/\nu$ that often are in the range $1300 < Re < 3300$, where U_b is the mean velocity, D the pipe diameter, and $\nu = \mu/\rho$ the kinematic viscosity. The laminar–turbulent transition occurs at $Re_c \approx 2300$ suggesting that collector pipes operate under both laminar and unsteady flow conditions.

For smooth pipes at turbulent conditions, $Re > Re_c$, the convective resistance is already small compared to the total borehole resistance, so fins provide limited overall efficiency gains. At laminar conditions $Re < Re_c$, however, convection accounts for about 50% of the total borehole resistance, offering the greatest potential for improvement. Excessive friction losses must also be avoided: if the friction factor increases by more than about 10% compared to smooth pipes, overall efficiency may decrease since pumping power scales as $P \propto f U_b^3$ and $U_b \propto Re$. Minimizing f at high Re is therefore essential.

A suitable fin configuration should thus promote transition to unsteady flow at $Re < Re_c$, thereby reducing convective heat-transfer resistance, while avoiding a significant increase in friction factor at $Re > Re_c$. This study aims to identify fin designs that satisfy both requirements. Although the thermohydraulic performance of finned pipes has been widely studied, most investigations focus on fully laminar or turbulent regimes [9, 11, 12]. In contrast, the present work targets the transitional regime, where the constraint of low friction factor (especially at $Re > Re_c$) rules out many conventional designs employing large fins ($O(0.1D)$). Such fins typically induce substantially higher pressure losses than micro-fins ($O(0.01D)$) [9, 13, 14]. To the authors' knowledge, internal fins explicitly designed under these combined constraints have not been previously assessed.

Experiments in the transitional Reynolds number regime are highly sensitive to inlet and initial conditions, making direct comparison across experimental configurations and with simulations difficult [15]. Moreover, available experimental data in this regime are sparse and often subject to significant uncertainties (typically 10 – 20%), with most studies focusing on mixed rather than forced convection [16]. A possible way to mitigate these ambiguities is to employ Direct Numerical Simulation (DNS) that provides precise control over boundary conditions, inlet disturbances, and flow development. DNS also circumvents the need for turbulence models, which are known to perform poorly in transitional flows. However, due to the very high computational cost of DNS, this method is impractical for full-scale GHE simulations. Instead, DNS on representative pipe sections can be carried out at a reasonable computational cost to analyse the influence of fins on the flow dynamics and obtain accurate heat transfer and pressure drop data. Such data can subsequently be used to develop more general models/correlations for system-level GHE analyses.

In this work, we use fully resolved DNS to accurately evaluate the performance of pipes with internal fins. The goal is to identify fin designs that promote unsteady flow at $Re < Rec$ while avoiding significantly higher f at $Re > Re_c$. The simulations are also used to quantify the thermohydraulic performance of such pipes in terms of heat transfer rate and pressure drop. Three continuous fin strategies are first examined: axial straight fins, continuous helical fins, and alternating helical fins. We then assess the effects of fin size, number, and twist rate on thermohydraulic performance. Based on these results, a promising fin design is selected and compared with a smooth pipe over the range $1300 < Re < 3300$ and brine Prandtl numbers $20 < Pr < 75$.

2. Methodology

We study, using Direct Numerical Simulations (DNS), fully developed flow in circular pipes, with and without surface modifications (fins). DNS is a model-free Computational Fluid Dynamics (CFD) approach in which the governing conservation equations for fluid flow and heat transfer are solved with sufficient spatial and temporal resolution to capture all relevant scales of motion without relying on turbulence or heat-transfer models. In this sense, DNS yields a reliable and accurate depiction of the flow by resolving all relevant dynamical scales directly from first principles. This method is particularly suitable in the transitional flow regime considered here where turbulence and heat transfer models are generally not reliable at predicting neither the onset of turbulence nor the effects of the turbulence on the flow and heat transfer. The main limitation of DNS is its substantial computational cost, since adequately resolving all relevant scales demands very fine grids and small time steps. To reduce the computational cost and complexity of the problem we make the following assumptions.

Since collector pipes are hundreds of meters long while fully developed flow typically occurs within the first 10 m [17], entrance effects are neglected, and a representative section with periodic boundary conditions in the axial x-direction is used. The analysis focuses on the convective heat transfer in the brine and excludes heat transfer through the pipe wall and the surrounding ground. Since the temperature difference between the pipe inner wall and the brine at a given streamwise location rarely exceeds 5°C, fluid properties (viscosity, density, specific heat and thermal conductivity) are assumed constant, and temperature is treated as a passive scalar. Although larger temperature variations may occur during shorter transients (for example when switching from heating to cooling operations) we believe the assumption of negligible brine temperature variations is a reasonable approximation for most operating conditions.

2.1. Numerical framework

The pipe in the computational domain has diameter D and length L. The wall boundary conditions are no slip $\boldsymbol{u} = 0$ and constant wall temperature $T_w > T_b$ where the bulk temperature is defined as $T_b = \Omega_l^{-1} \int_{\Omega l} Tu d\Omega$, the Ω_l is the liquid volume in the pipe and u is the axial velocity component. To generalise the problem and to identify the governing non-dimensional parameters of our problem, we make all variables non-dimensional using the pipe diameter D, bulk velocity $U_b = \Omega_l^{-1} \int_{\Omega l} u d\Omega$ and liquid density as ρ. The non-dimensional variables are $x_i^* = x_i/D$, $u_i^* = u_i/U_b$, $t^* = tU_b/D$, $p^* = p/(\rho U_b^2)$. The non-dimensional temperature is defined as $T^* = (T - T_b)/(T_w - T_b)$ that gives a $T_w^* = 1$ and $T_b^* = 0$. The asterisk notation "*" is hereafter omitted for brevity. By substituting the non-dimensional variables into the governing equations for the fluid- and thermodynamics (conservation of mass, momentum and energy) the governing equations take the following non-dimensional form

$$\boldsymbol{\nabla} \cdot \boldsymbol{u} = 0\,, \tag{1}$$

$$\frac{\partial \boldsymbol{u}}{\partial t} + (\boldsymbol{u} \cdot \boldsymbol{\nabla})\boldsymbol{u} = -\boldsymbol{\nabla} p + \frac{1}{Re}\boldsymbol{\nabla} \cdot (\boldsymbol{\nabla u} + \boldsymbol{\nabla u}^T) + \boldsymbol{a} = 0, \tag{2}$$

$$\frac{\partial T}{\partial t} + \boldsymbol{u} \cdot \boldsymbol{\nabla} T = \frac{1}{RePr}\boldsymbol{\nabla}^2 T + S_Q, \tag{3}$$

where $\boldsymbol{u}$ is the velocity field, p the pressure, $\boldsymbol{a}$ is a uniform axial body force maintaining a constant and specified flow rate (equivalent to imposing a constant axial pressure gradient), T the liquid temperature, and S_Q a uniform cooling term ensuring a constant bulk temperature and axial periodicity of the temperature field. As indicated by the non-dimensional governing equations (and by Reynolds' law of similarity), the flow and heat transfer in a given pipe geometry is fully described by the Reynolds number $Re = U_b D/\nu$ and the Prandtl number $\mathrm{Pr} = c_p \mu/k$, where c_p is the specific heat and k the thermal conductivity. This implies that the hydro- and thermodynamics is the same for any geometrically similar pipe with the same Re and Pr. In the present problem, Re may be interpreted as the non-dimensional flow rate for a given pipe and brine. The Pr can similarly be interpreted as inversely proportional to the thermal diffusivity of that brine.

Table 1 shows that relevant parameter ranges are approximately $400 < Re < 7000$ and $20 < Pr < 75$. As outlined in section 1, our main goal in introducing fins is to promote unsteady flow below the critical Reynolds number Re_c, thereby enhancing heat transfer where smooth pipes remain laminar, without substantially increasing the friction factor f above Re_c. We therefore focus on $1300 \leq Re \leq 3300$, where fins are expected to induce unsteady flow. Below this range, the flow most likely remains laminar even with fins, while far above Re_c the flow is fully turbulent and smooth pipes already provide high heat transfer. This interval also enables evaluation of the pressure-drop increase under conditions where both smooth and finned configurations are turbulent.

The governing equations (1) to (3) are solved using the open-source, finite-volume and tree-based grid code Basilisk (basilisk.fr). The bulk velocity U_b is maintained by applying a time-dependent but spatially uniform acceleration term a_x in (2) (determined using a PI-controller) that plays the same role as an applied axial pressure gradient. At steady flow conditions, the total forcing $F_a = \Omega_l \rho a_x$ exactly balances the wall shear stress $F_w = \tau_w \pi D L$. The equivalent pressure drop over the pipe length L is $F_a = \pi(D/2)^2 \Delta p$ that gives $\Delta p/L = \rho a_x$ (with a liquid volume $\Omega_l = \pi(D/2)^2 L$). Using the definition of the Darcy friction factor f as $\Delta p = f(L/D)(\rho U_b^2/2)$ then gives $f = 2a_x D/U_b^2$. The same methodology is used in the energy equation (3) where S_Q is varied uniformly (with another PI-controller) to force $T_b = 0$, similarly to methodology of [19]. At statistically steady conditions, the total cooling rate $Q_c = \Omega_l S_Q$ equals the total wall heat flux $Q_w = q_w \pi D L$. The wall heat flux is thus $q_w = S_Q D/4$. With the convective heat transfer coefficient $h = q_w/(T_w - T_b)$ we further define the non-dimensional Nusselt-number as $Nu = hD/k$ that represents the ratio of convective to conductive heat transfer rate.

For a fully developed laminar flow in smooth circular pipes of radius $R = D/2$, the axial velocity profile is $u(r) = 2(1-(r/R)^2)$, where r is the radial coordinate from the pipe centre. With the uniform cooling term S_Q, the temperature profile becomes $T(r) = RePr(S_Q/4)(R^2 - r^2) + T_w$ and by maintaining a constant bulk temperature $T_b = (\pi R^2)^{-1}\int_0^R Tu2\pi r\,dr$, we get the analytical solution $Nu_{smooth,lam} = 6$ for laminar flow in smooth pipes with a uniform cooling term.

It should be noted that the value $Nu_{smooth,lam} = 6$ differs from the classical result $Nu \approx 3.66$, which applies to smooth pipes under laminar flow with a constant wall temperature and no cooling term. In that classical case, the bulk temperature gradually approaches the wall temperature along the pipe, making periodic axial boundary conditions infeasible. Due to the high computational cost of DNS, a short periodic domain is required here. Nonetheless, this approach yields heat transfer rates suitable for relative comparison and consistent with experimental correlations and non-periodic simulations in the unsteady flow regime [19].

The transition to turbulence in smooth pipes occurs near $Re_c \approx 2300$, though it can vary between $2000 \lessapprox Re \lessapprox 4000$ depending on inlet conditions, wall roughness, and disturbances. In geothermal collector systems, turbulence is promoted by pumps, wall imperfections, and pipe bends. To replicate these effects, simulations begin at $Re = 3300$ and 2300, where turbulence is guaranteed, and then proceed through decreasing Reynolds numbers $Re = (3300, 2300, 2050, 1950, 1800, 1700, 1300)$. After each step, the flow is allowed to reach a statistically steady, fully developed state before further reduction. This ensures each case evolves from a realistic unsteady flow until laminar conditions are achieved (i.e., all velocity fluctuations vanish). The instantaneous Nu and f are time-averaged over the fully developed regime until convergence is obtained.

Table 1. Typical brines (water solutions) used in geothermal heat collector systems and their material parameters obtained from [18]. All properties are evaluated at an operating temperature of 0°C. A pipe inner diameter of D = 40 mm and flow rates Q = 0.1–0.7 L/s are used to compute the non-dimensional Reynolds number $Re = U_b D\rho/\mu$ and the Prandtl number $Pr = c_p\mu/k$. The values show that the relevant ranges of the non-dimensional parameters are approximately $400 < Re < 7000$ and $20 < Pr < 75$.

Brine	C_a [wt-%]	ρ [kg/m³]	c_p [J/(kg·K)]	k [W/(m·K)]	μ [mPa·s]	Pr [–]	Re [–]
Potassium carbonate	30	1307	2932	0.536	4.29	23	970–6790
Ethylene glycol	30	1046	3677	0.447	4.31	36	771–5400
Ethanol	29	967	4193	0.403	6.40	67	481–3365
Propylene glycol	33	1035	3852	0.416	8.17	76	403–2820

2.2. Grid study and validation

The computational domain is discretised in space using the finite volume method. To accurately resolve all relevant hydro- and thermodynamic scales (that is a prerequisite for DNS) this discretisation needs to be sufficiently fine. We first verify that the numerical grid resolves all relevant scales, ensures grid convergence, and agrees with experimental correlations (further comparisons are presented in section 3). The case $Re = 3300$ is considered the most demanding numerically and is therefore used for validation. A smooth pipe is selected to enable direct comparison with established correlations.

The base grid consists of cubic cells with side length $\Delta = D/58$ in the core and a refined wall region of about 10 cells with $\Delta = D/116$. This yields $y^+ = yu_\tau/\nu \approx 1$ for the wall-adjacent cell, satisfying DNS requirements for wall-bounded turbulence. In the near-wall region, the grid ratio $\Delta/\eta = 1.4$ (with $\eta = (\nu^3/\varepsilon)^{1/4}$ and $\varepsilon = U_b a_x$) remains below the DNS criterion $\Delta/\eta \lessapprox 2.1$ for isotropic turbulence [20], ensuring adequate resolution of the smallest turbulent scales. Since Pr > 1, even smaller thermal scales may occur near the wall. To account for this, an additional refinement layer of about 10 cells with $\Delta = D/232$ is included at the wall. The friction factor f from both the base and refined grids was compared with the correlation of [21] for turbulent pipe flow expressed as

$$\frac{1}{\sqrt{f_{Haaland}}} = -1.8 log_{10}\left[\left(\frac{\varepsilon/D}{3.7}\right)^{1.11} + \frac{6.9}{Re}\right], \tag{4}$$

where we use the value $\varepsilon/D = 10^{-5}$ corresponding to smooth pipes. This comparison shows excellent agreement ($f_{Haaland} = 0.043$ and $f_{\mathrm{DNS}} = 0.0432$ with the base grid) and only a 1% decrease with the refined grid. The predicted Nusselt numbers for $Pr = (20,\ 40,\ 75)$ are then compared with the experimental correlations by [16] and [17] given by

$$Nu_{Gni} = \frac{(f/8)(Re-1000)Pr}{1+12.7\sqrt{f/8}\left(Pr^{2/3}-1\right)}, \quad (5)$$

$$Nu_{Meyer} = 0.041 Re^{1.117} Pr^{1/3} f. \quad (6)$$

Our DNS with the base grid gives $Nu_{DNS} = 42, 51, 58$ and the correlations $Nu_{Meyer} = 41, 51, 63$ and $Nu_{Gni} = 36, 45, 56$ for Pr = 20, 40, 75, respectively. This is deemed a good agreement considering that the expected accuracy is approximately ±20% at this relatively low Re in the transitional flow regime [16]. The relative deviation predicted by our DNS using the refined to the base grid increases slightly with Pr as 0% at Pr = 20, 1% at Pr = 40, and 6% at Pr = 75. Since the case Re = 3300, Pr = 75 represents the most demanding condition numerically, the expected error using the base grid is estimated below 5% for all other cases. This accuracy is considered sufficient, and the base grid is used for all subsequent simulations. Further comparison between predicted f and Nu with analytical and experimental correlations are performed for a range of Re spanning the laminar to turbulent transition region in figure 6 with good agreement, further validating our numerical setup.

3. Results

We first evaluate three fin design strategies in section 3.1, then focus on the most promising concept to examine the effects of fin size, number, and twist rate on heat transfer and pressure drop (section 3.2). Then, we compare the thermohydraulic performance of a selected design with that of a smooth pipe (section 3.3).

3.1. Evaluation of fin design concepts

As noted in section 1, an effective fin design should promote transition to unsteady flow at $Re < Re_c$ while avoiding large increases in friction at $Re > Re_c$. Since fins inherently increase f, we focus on designs primarily aligned with the flow direction, as transverse fins tend to cause greater frictional losses.

Three fin concepts are evaluated: (i) straight fins aligned with the pipe axis, (ii) continuous helical fins, and (iii) fins with alternating helical orientations. Illustrations of one axial period of each design are shown in figure 1. All configurations use n_{fin} = 16 equally spaced fins with height h_{fin} = 0.6 mm and width of $2h_{fin}$. Preliminary tests indicate these dimensions cause minimal friction increase at $Re > Re_c$ while promoting unsteady flow at $Re < Re_c$. The pipe has an inner diameter D = 40 mm and lengths of L = 8.8D, 17.5D, and 35D for the straight, continuous, and alternating helical fins, respectively, corresponding to a twist rate of ω_{fin} = 360° per 17.5D for the two latter concepts. The shorter straight-fin pipe length reduces computational cost while still resolving the relevant unsteady flow scales. For clarity, figure 1d is shown compressed to L = 17.5D.

Simulations begin at Re = 2300, where all designs produce unsteady flow. The Reynolds number is then gradually reduced until the flow becomes laminar, indicated by decaying velocity fluctuations and Nu and f approaching analytical laminar values. As shown in figure 2, transition to laminar flow occurs at Re = 2050 for straight fins, Re = 1950 for continuous helices, and Re = 1700 for alternating helices. Thus, the alternating helical fins trigger unsteady flow at substantially lower Re than the other designs. Examples of the instantaneous flow fields are shown in figure 2 for the straight and alternating fins at Re = 2050 where the former fins give a laminar flow while the latter maintains an unsteady flow state. The friction factor is however within a few percent of (4) (valid for smooth pipes) at Re = 2300 for all concepts. Moreover, all unsteady flow cases yield Nu values about 5 times higher than their laminar counterparts highlighting the importance of maintaining an unsteady flow for efficient heat transfer. Hence, the alternating helical design is selected for further parametric analysis of fin size, number, and twist rate.

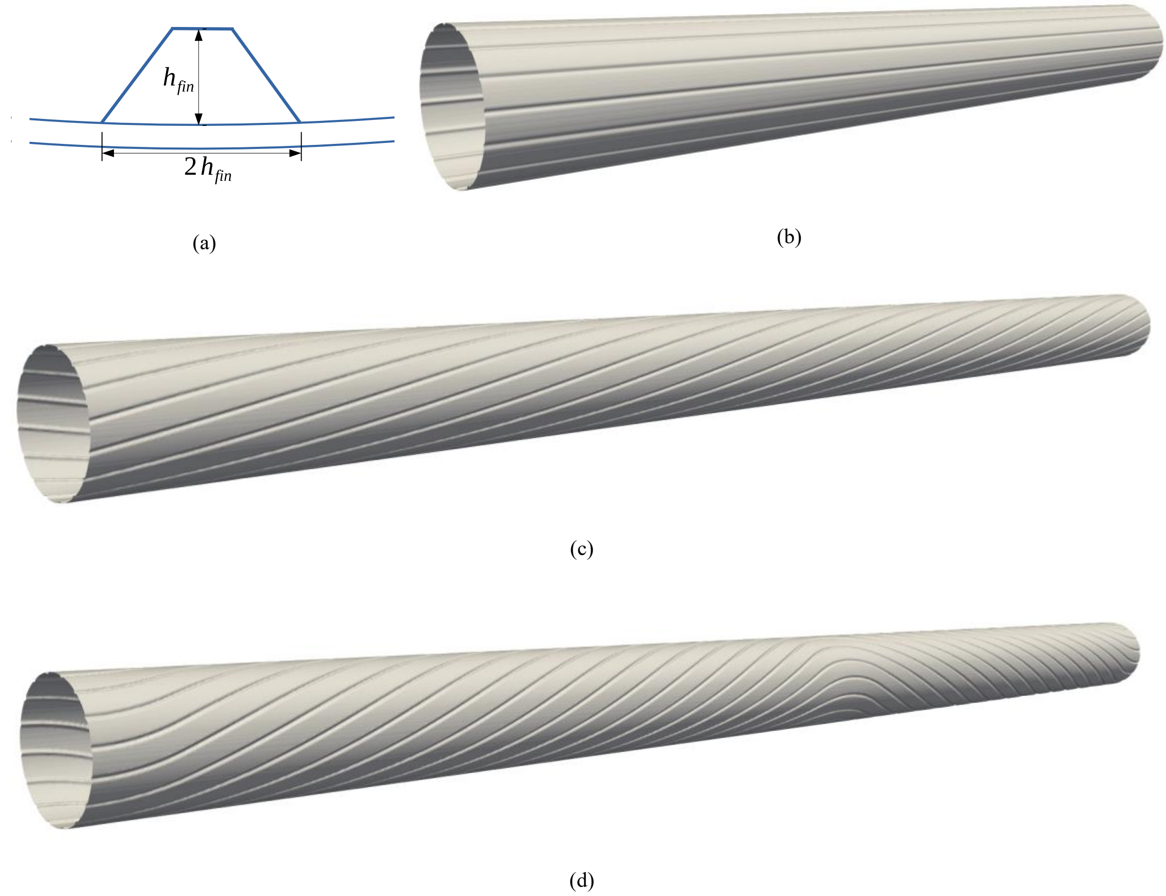

Figure 1: (a) Schematic of the fin cross-section used in all fin designs. The three evaluated fin design concepts: (a) Straight fins along the pipe. (b) Fins continuously rotating along the pipe (one full revolution shown here). (c) Fins with alternating helical direction along the pipe (pipe length scaled to half its actual length).

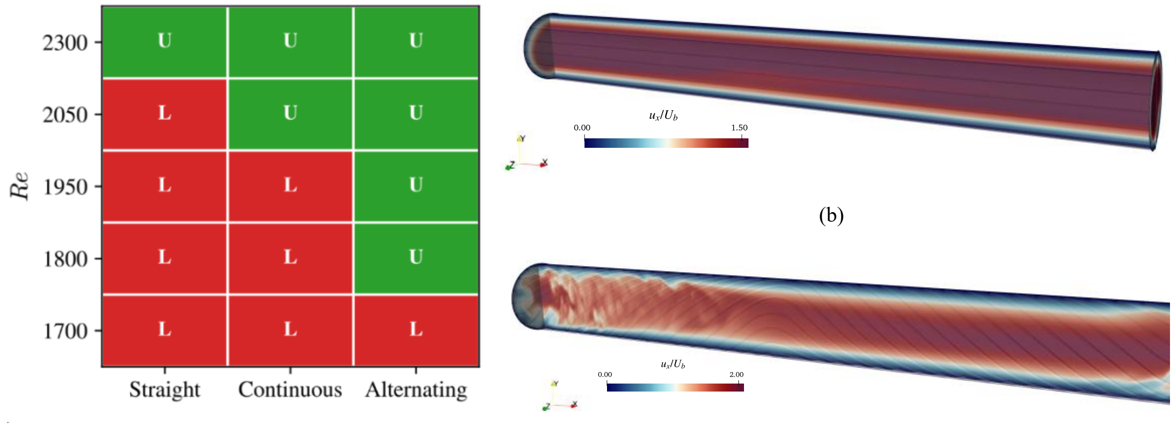

(a)

(c)

Figure 2: (a) Steady-state flow type at various Reynolds numbers for the straight, continuous helical, and alternating helical fin concepts. Simulations start at Re = 2300 where all concepts show an unsteady flow (U) and Re is gradually reduced until laminar flow (L) is reached. (b) Non-dimensional axial velocity for that case with straight fins at Re = 2050 that decays to a laminar flow. (c) Non-dimensional axial velocity for that case with alternating helical fins at Re = 2050 that maintains an unsteady flow. Here, the pipe length is scaled to 1/4 of its actual length.

3.2. Parametric study on alternating helical fin configurations

In this section, the effects of fin size, fin number, and twist rate on the thermohydraulic performance of the alternating helical fin design are evaluated.

The effect of the fin height h_{fin} is evaluated for the alternating helical fin design at Re = 3300, where the flow is fully turbulent, to identify when f becomes excessively high relative to a smooth pipe. As shown in figure 3a, the DNS results agree well with the smooth pipe correlation by Haaland [21] at h_{fin} = 0. However, f rises sharply for $h_{fin} \gtrsim$ 1 mm, reaching 18% above the smooth case at 1.8 mm. A fin height of $\sim$ 1 mm or less thus offers a good balance between heat transfer and pressure loss. In subsequent simulations, we use h_{fin} = 0.6 mm, where f remains close to that of a smooth pipe for $Re > Re_c$.

We next examine how the number of fins affects the ability to trigger unsteady flow at $Re < Re_c$. Using the alternating helical design with $L = 35D$ and h_{fin} = 0.6 mm, we vary the number of equally spaced fins n_{fin} = (2, 16, 24, 32). As $n_{fin} \rightarrow 0$ or ∞, the geometry approaches a smooth pipe, suggesting an optimal finite value. For each case, simulations start at Re = 2300 and Re is successively lowered until laminar flow occurs. The results are shown in figure 3b and indicate that n_{fin} > 16 offers no advantage for inducing unsteady flow, while even n_{fin} = 2 significantly alters the flow compared to a smooth pipe. Thus, $n_{fin} \leq 16$ is a suitable choice. The Nu and f values for all unsteady cases are within a few percent of the corresponding n_{fin} = 16 cases, indicating that the primary role of the fins is to trigger unsteady flow rather than directly increase heat transfer proportional to n_{fin}.

Finally, we assess how the fin twist rate ω_{fin} affects the ability of the alternating helical design to induce unsteady flow at $Re < Re_c$. The geometry is kept constant as $L = 35D$, h_{fin} = 0.6 mm, and n_{fin} = 16, while ω_{fin} is varied so that the fins rotate clockwise by ω_{fin} over $0 \leq x < L/2$ and counterclockwise over $L/2 \leq x \leq L$. The tested twist rates are ω_{fin} = (0°, 30°, 45°, 180°, 360°), as shown in figure 4. Results indicate that $\omega_{fin} \gtrsim 45°$ is sufficient to maintain unsteady flow down to $1700 < Re < 1800$, comparable to the fully twisted case (360°). For ω_{fin} = 30°, the unsteady flow decays earlier, approaching the behaviour of the straight fin case (0°), which becomes laminar at $2050 < Re < 2300$.

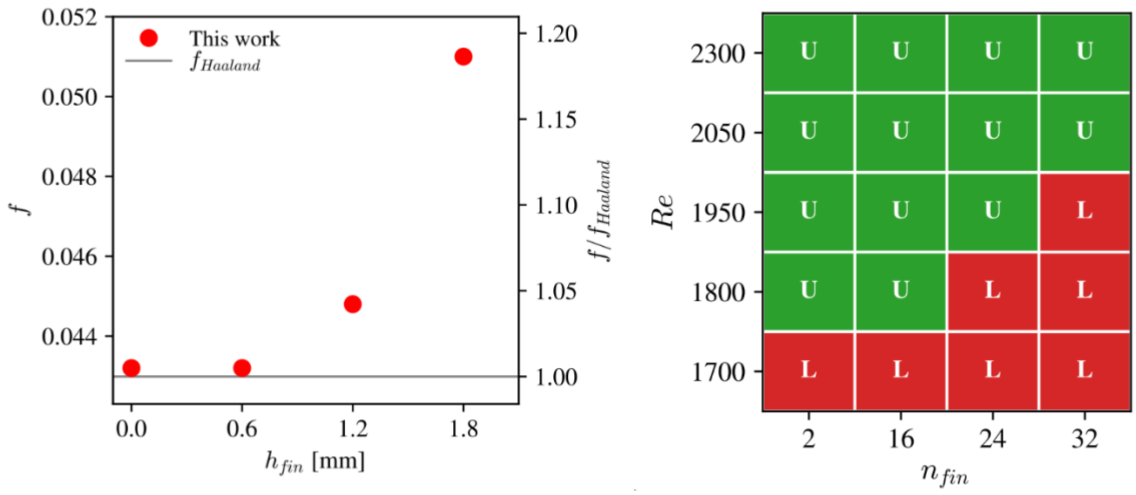

(a)

(b)

Figure 3: (a) Friction factor predicted by DNS of the alternating helical fin design at Re = 3300 for various fin heights h_{fin}. The h_{fin} = 0 case (smooth pipe) aligns well with the friction factor correlation of [21] developed for turbulent flow in smooth pipes. The results suggests that h_{fin} = 0.6 mm is a suitable choice where f remains close to that of a smooth pipe. (b) Flow regimes at steady state for the alternating helical fin design with h_{fin} = 0.6 mm, shown for different Reynolds numbers Re and numbers of equally spaced fins n_{fin}. Simulations start at Re = 2300, where all cases are unsteady (U), and Re is gradually decreased until laminar flow (L) is reached. Here, n_{fin} = 16 is considered a reasonable choice with unsteady flow obtained until at least Re = 1800.

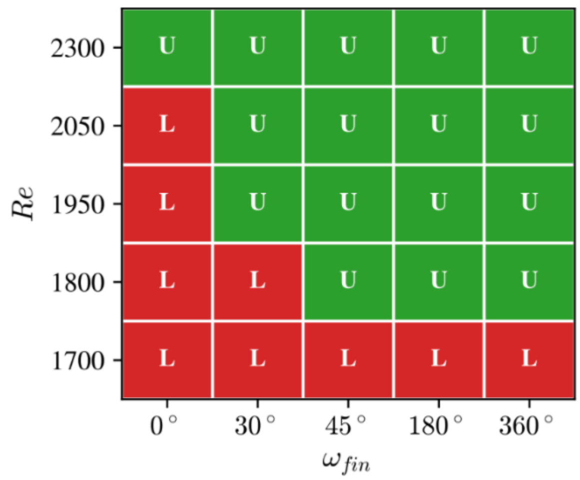

Figure 4: Steady state flow type observed for different Re-numbers and fin twisting rates ω_{fin} for the alternating helical fin design. The simulations are started at Re = 2300, where all designs show an unsteady flow, and then Re is successively reduced until the flow becomes laminar.

3.3. Thermohydraulic evaluation of promising alternating helical fin design

Based on the results from the parametric study, we consider a promising alternating helical fin design with the parameters L = 35D, h_{fin} = 0.6 mm, n_{fin} = 16 and ω_{fin} = 360°. This promising design is compared with smooth pipe DNS (L = 8.8D) and experimental correlations. Here, we consider brines with $\mathrm{Pr} = (20, 40, 75)$ and at flow rates corresponding to $Re = (3300, 2300, 2050, 1950, 1800, 1700, 1300)$.

Non-dimensional temperature contours from the DNS of the alternating helical fin design are shown in figure 5. For $Re = 3300–1800$, the unsteady flow promotes strong thermal mixing and thin boundary layers, which thicken gradually as Re decreases. At $Re \leq 1700$, the flow becomes laminar, and heat transfer occurs mainly by diffusion, resulting in much thicker boundary layers.

In comparison, the smooth pipe exhibits turbulent flow at $Re \geq 2300$ but transitions to laminar at $Re \leq 2050$. The alternating helical fin design, however, maintains unsteady regions even below this threshold. These localized unsteady zones, advected along the pipe, intermittently disturb the thermal boundary layer and enhance local convective heat transfer. The resulting effects on the overall pressure drop and heat transfer are quantified in figure 6.

Figure 6a shows the friction factor versus Re alongside the laminar solution for smooth pipes ($f = 64/Re$) and the correlation by [21]. The smooth pipe DNS agrees closely with both, confirming the numerical accuracy. For the alternating fin design, transition to unsteady flow occurs earlier (1700< Re<1800) compared to the smooth pipe (2050< Re<2300), while the friction factor remains only slightly higher outside the intermediate region 1700< Re<2300.

A similar trend appears in figure 6b, where the alternating fin design achieves 300–600% higher heat transfer in the intermediate region ($1700 < Re < 2300$). For $Re \leq 1700$, both geometries approach the laminar smooth-pipe value for our setup (Nu = 6), with the finned pipe showing 1–8% enhancement. At $Re \geq 2300$, differences are within 5%, and both cases align well with the correlation by [16]. Interestingly, the latter correlation, developed for smooth pipes, can predict Nu for the finned pipe within 10% margin all the way down to Re = 1800. However, the correlation by [22] is only within approximately 15% of our DNS at Re > 3000 which is also the lower range of validity for that correlation.

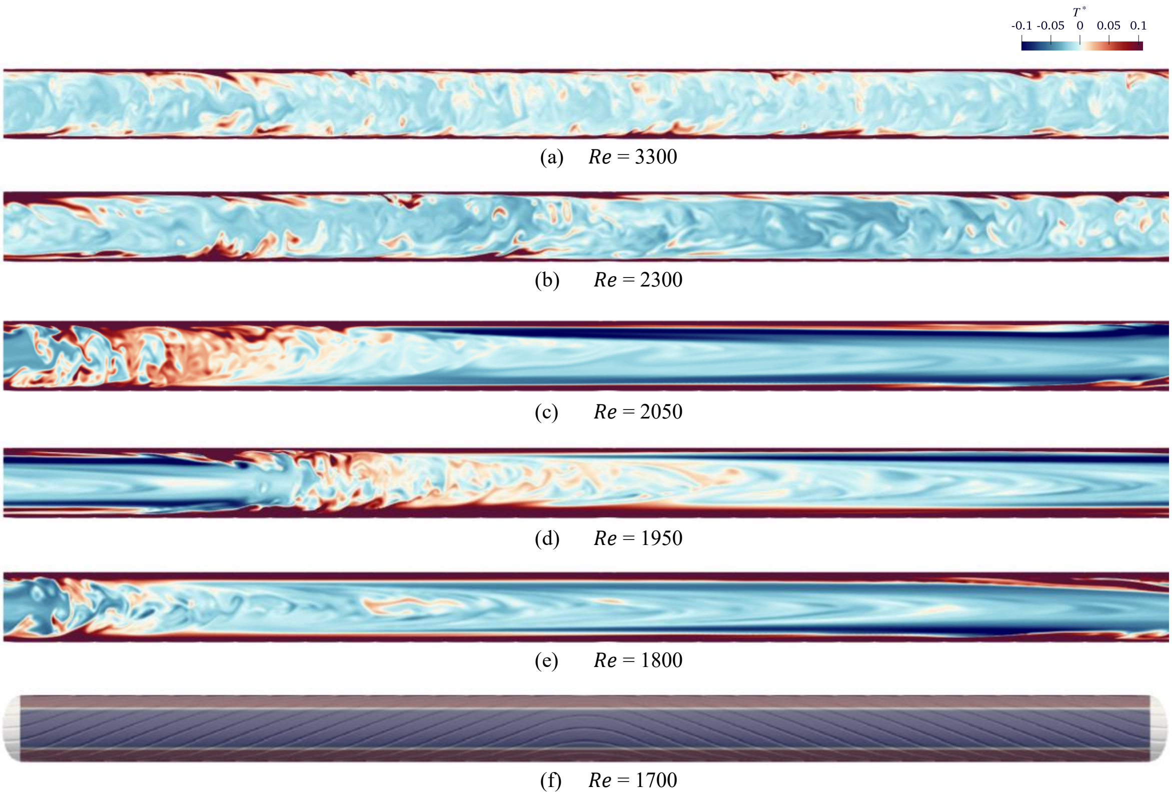

Figure 5: Non-dimensional temperature contours $T^* = (T - T_b)/(T_w - T_b)$ at the plane $z = 0$ from the DNS of alternating helical fin pipe for Pr = 75. The Reynolds number decreases from 3300 to 1700, where the flow becomes laminar. Consequently, or Re < 1700, the flow and temperature fields remain identical to the Re = 1700 case. The pipe is shown at half its actual length ($L/2 = 17.5D$) for clarity, and the temperature scale is the same for all panels as in (a).

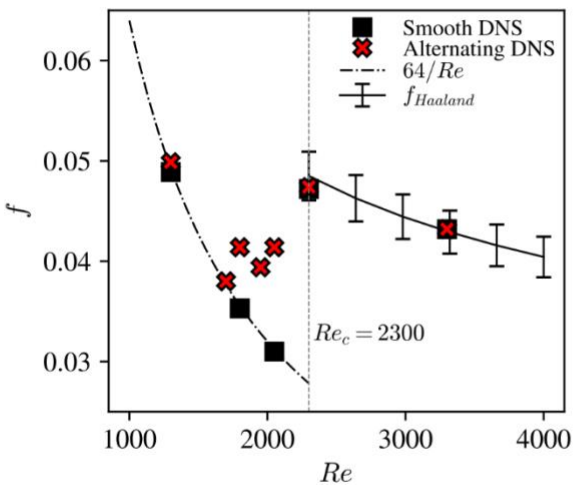

(a)

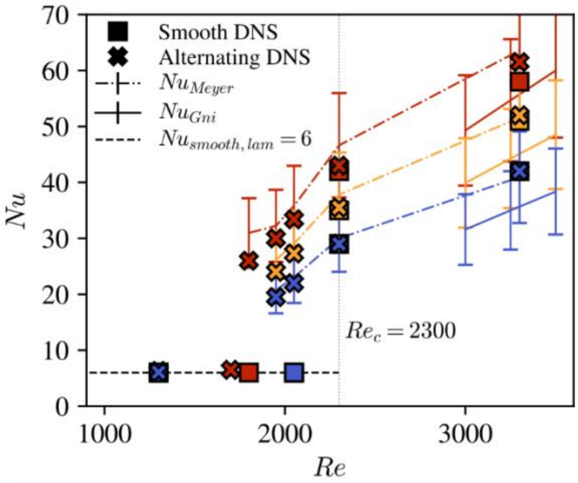

(b)

Figure 6: Time-averaged DNS results for the alternating helical fin design ($L = 35D$, h_{fin} = 0.6 mm, n_{fin} = 16, ω_{fin} = 360°) compared with a smooth pipe. (a) Friction factor versus Re, including the analytical laminar solution for smooth pipes ($f = 64/Re$) and the correlation by [21] (±5%). The smooth pipe agrees well with theory, while the finned pipe transitions to unsteady flow at lower Re. (b) Nusselt number versus Re, compared with the derived laminar solution for smooth pipes in our setup (Nu = 6), the correlation by [22] ±20% (calculated using f from (4)) for Re > 3000, and [16] ±20% using f from the DNS. The red, orange and blue colours represent the cases with Pr = 75, 40, 20, respectively. The earlier unsteady transition for the finned design yields 300–600% higher Nu in the range 1700<Re<2300.

4. Conclusions

Fully resolved Direct Numerical Simulations (DNS) were conducted to assess the thermohydraulic performance of finned and smooth pipes under conditions relevant to geothermal heating systems ($1300 \leq Re \leq 3300$, $20 \leq Pr \leq 75$). Among the tested configurations, the alternating helical fin design proved most effective in promoting unsteady flow at subcritical Reynolds numbers (Re < 2300). Parameter studies show that a fin height of ≤ 1 mm provides a favourable balance between heat transfer and pressure drop, while more than 16 fins offer no additional benefit. A twist rate of at least 45° over half the pipe length ($L/2 = 17.5D$) is sufficient to sustain unsteady flow down to $Re \approx 1800$. The alternating helical fin design enhances heat transfer by 300–600% compared to a smooth pipe within the intermediate Reynolds number range $1700 < Re < 2300$, with only a marginal (≤ 2%) increase in friction factor outside this range. The performance evaluation thus suggests that alternating helical fins can achieve superior thermohydraulic performance in the intermediate Reynolds number range and similar (or slightly better) performance as that of a smooth pipe outside of this region.

A quantitative assessment of the net system-level benefit, accounting for the trade-off between reduced borehole thermal resistance, pumping power, and heat-pump efficiency, requires development of correlations and coupling the present results with full GHE and heat-pump models. This is left for future work. Future work could also include experimental validation of the proposed fin designs, through both controlled laboratory heat-extraction experiments and field-based Thermal Response Testing, while accounting for the inherent uncertainties associated with the latter measurements [23, 24].

Acknowledgements

We acknowledge funding from MouviTech Sweden AB.

References

[1] Aminhossein Jahanbin. Thermal performance of the vertical ground heat exchanger with a novel elliptical single u-tube. Geothermics, 86:101804, 2020.

[2] Jeffrey D Spitler, Saqib Javed, and Randi Kalskin Ramstad. Natural convection in groundwater-filled boreholes used as ground heat exchangers. Applied Energy, 164:352–365, 2016.

[3] Göran Hellström. Ground Heat Storage, Thermal Analysis of Duct Storage Systems, I. Theory. PhD thesis, University of Lund, 1991.
[4] Saqib Javed and Jeffrey Spitler. Accuracy of borehole thermal resistance calculation methods for grouted single u-tube ground heat exchangers. Applied Energy, 187:790–806, 2017.
[5] Hossein Javadi, Seyed Soheil Mousavi Ajarostaghi, Mohsen Pourfallah, and Mohammad Zaboli. Performance analysis of helical ground heat exchangers with different configurations. Applied Thermal Engineering, 154: 24–36, 2019.
[6] M Roshani, MJ Hosseini, AA Ranjbar, and A Torbatinejad. Enhancing geothermal heat pump efficiency with fin creation and microencapsulated pcm: A numerical study. Journal of Energy Storage, 95:112664, 2024.
[7] Ralph L Webb and Nae-Hyun Kim. Principles of Enhanced Heat Transfer. Taylor & Francis, 2005.
[8] Mohamed H. Mousa, Nenad Miljkovic, and Kashif Nawaz. Review of heat transfer enhancement techniques for single phase flows. Renewable and Sustainable Energy Reviews, 137:110566, 2021.
[9] Wen-Tao Ji, Anthony M Jacobi, Ya-Ling He, and Wen-Quan Tao. Summary and evaluation on single-phase heat transfer enhancement techniques of liquid laminar and turbulent pipe flow. International Journal of Heat and Mass Transfer, 88:735–754, 2015.
[10] Yi-Ping Tu, Hsu-Te Lin, and Rong-Hua Yeh. Experimental study of fully developed turbulent flow in internally finned tubes. Journal of Enhanced Heat Transfer, 32, 2025.
[11] JP Meyer and SM Abolarin. Heat transfer and pressure drop in the transitional flow regime for a smooth circular tube with twisted tape inserts and a square-edged inlet. International Journal of Heat and Mass Transfer, 117:11 – 29, 2018.
[12] Gonçalo G Cruz, Miguel AA Mendes, Jos MC Pereira, H Santos, A Nikulin, and Ana S Moita. Experimental and numerical characterization of single-phase pressure drop and heat transfer enhancement in helical corrugated tubes. International Journal of Heat and Mass Transfer, 179:121632, 2021.
[13] Lin Liu, Ziyong Cao, Tong Shen, Ling Zhang, and Lin Zhang. Experimental and numerical investigation on flow and heat transfer characteristics of a multi-waves internally spiral finned tube. International Journal of Heat and Mass Transfer, 172:121104, 2021.
[14] Michael K Jensen and Alex Vlakancic. Technical note experimental investigation of turbulent heat transfer and fluid flow in internally finned tubes. International Journal of Heat and Mass Transfer, 42(7):1343 – 1351, 1999.
[15] Afshin J. Ghajar. Chapter one - heat transfer and pressure drop in the transition region of smooth horizontal circular tubes with different inlet configurations. In Ephraim M. Sparrow, John P. Abraham, John M. Gorman, and W.J. Minkowycz, editors, Advances in Heat Transfer, volume 51 of Advances in Heat Transfer, pages 1 – 53. Elsevier, 2019.
[16] Josua P Meyer, Marilize Everts, Nicole Coetzee, Kersten Grote, and M Steyn. Heat transfer coefficients of laminar, transitional, quasi-turbulent and turbulent flow in circular tubes. International Communications in Heat and Mass Transfer, 105:84 – 106, 2019.
[17] JP Abraham, EM Sparrow, and JCK Tong. Heat transfer in all pipe flow regimes: laminar, transitional/intermittent, and turbulent. International Journal of Heat and Mass Transfer, 52(3-4):557 – 563, 2009.
[18] Åke Melinder. Thermophysical properties of aqueous solutions used as secondary working fluids. PhD thesis, KTH, 2007.
[19] Sergio Pirozzoli, Joshua Romero, Massimiliano Fatica, Roberto Verzicco, and Paolo Orlandi. Dns of passive scalars in turbulent pipe flow. Journal of Fluid Mechanics, 940:A45, 2022.
[20] Stephen B Pope. Turbulent flows. IOP Publishing, 2001.
[21] S. E. Haaland. Simple and explicit formulas for the friction factor in turbulent pipe flow. Journal of Fluids Engineering, 105(1):89 – 90, 03 1983.
[22] Volker Gnielinski. Neue gleichungen für den wärme und den stoffübergang in turbulent durchströmten rohren und kanälen. Forschung im Ingenieurwesen A, 41:8 – 16, 1975.
[23] Saqib Javed and Jeffrey D Spitler. Vertical ground heat exchanger pressure loss – experimental comparisons and calculation procedures. Geothermics, 105:102546, 2022.
[24] Saqib Javed and Jeffrey D Spitler. Comparison of thermal performance and thermal resistance of two different types of single u-tube ground heat exchangers. In International Heat Transfer Conference Digital Library. Begel House Inc., 2023.